Treatment of non-sparse cratering in planetary surface dating

T. Kneissl ∗, G.G. Michael, N. Schmedemann
Institute of Geological Sciences, Planetary Sciences and Remote Sensing, Freie Universität Berlin, Malteserstr. 74-100, 12249 Berlin, Germany

Abstract
We here propose a new technique to derive crater size-frequency distributions (CSFDs) from non-sparsely cratered surfaces, by accounting for the loss of craters due to subsequent crater/ejecta coverage. This approach, which we refer to as the buffered non-sparseness correction (BNSC), relates each crater to a measurement area found by excluding regions in the study area that have been resurfaced by larger craters and their ejecta blankets. The approach includes the well-known buffered crater counting (BCC) technique in order to consider the potential identification of craters whose centers are located outside the counting area. We demonstrate the new approach at two test sites on the Moon, one on the ancient lunar highlands outside the South Pole Aitken basin and the other on the much younger surface of lunar Mare Serenitatis. As expected, the correction has a much stronger effect on ancient, densely cratered surfaces than on younger, sparsely cratered surfaces. Furthermore, these first results indicate that the shapes of CSFDs on ancient terrains are actually very similar to the shapes of CSFDs on younger terrains.

1. Introduction

The use of crater size-frequency distributions (CSFDs) for detemination of relative and absolute surface ages is a well-established and frequently applied method in the planetary community (e.g., Öpik, 1960 ; Baldwin, 1964 ; Neukum, 1983).

The area occupied by craters and their ejecta on a counting area has customarily been considered negligible when consider- ing crater densities. The assumption holds well when the densi- ties are low. As they increase, it generally continues to hold for craters at the large end of the size–frequency distribution, but be- gins to break down for craters at smaller sizes: their measured spatial densities are relatively diminished because a fraction of the accumulated population has been obliterated by superposed larger craters. In this paper we consider an approach to studying crater populations which does not require this assumption.

We refer to the situation using the term non-sparseness because it is relevant whenever the area occupied by craters and their ejecta becomes non-negligible. Although this is unquestionably the case for densely cratered surfaces, it should be noted that the on- set of non-sparseness occurs well before what might normally be considered as dense cratering.

If a surface becomes non-sparsely cratered, the ejecta blan- kets of impact craters act like new geologic units that superpose the older, preexisting crater population. Including their areas and crater statistics is comparable to including other geologic units into the counting area (Warner et al., 2015). This contradicts the requirement for a crater count to be based on the use of homoge- neous geological units (e.g., Wilhelms et al., 1987). Craters superposed on the ejecta blankets of larger craters only carry information about the formation age of the respective crater they superpose, not about the age of the larger geologic unit. Consequently, craters superposed on ejecta blankets can only be used for age de- terminations of the ejecta blanket itself.

As a consequence, age determinations on non-sparsely cratered units become problematic because the “loss” of small craters from the original cratering record complicates the interpretation of the CSFD. To remove this effect, we propose a new approach for de- riving CSFDs from crater measurements on a non-sparsely cratered geologic unit.

2. Correcting non-sparse crater distributions

The derivation of a CSFD requires the number of impact craters to be normalized to a measurement area (Arvidson, 1979). In the traditional crater-counting approach this includes all impact craters whose centers are located inside a defined area, which should rep- resent a homogeneous geologic unit. Here, the area assigned to each crater is identical, i.e.:

$$A_T = A_U$$

where A_T is the reference area assigned to a crater in the tradi- tional crater counting approach and A_U is the area of the geologic unit of interest (Fig. 1 A).

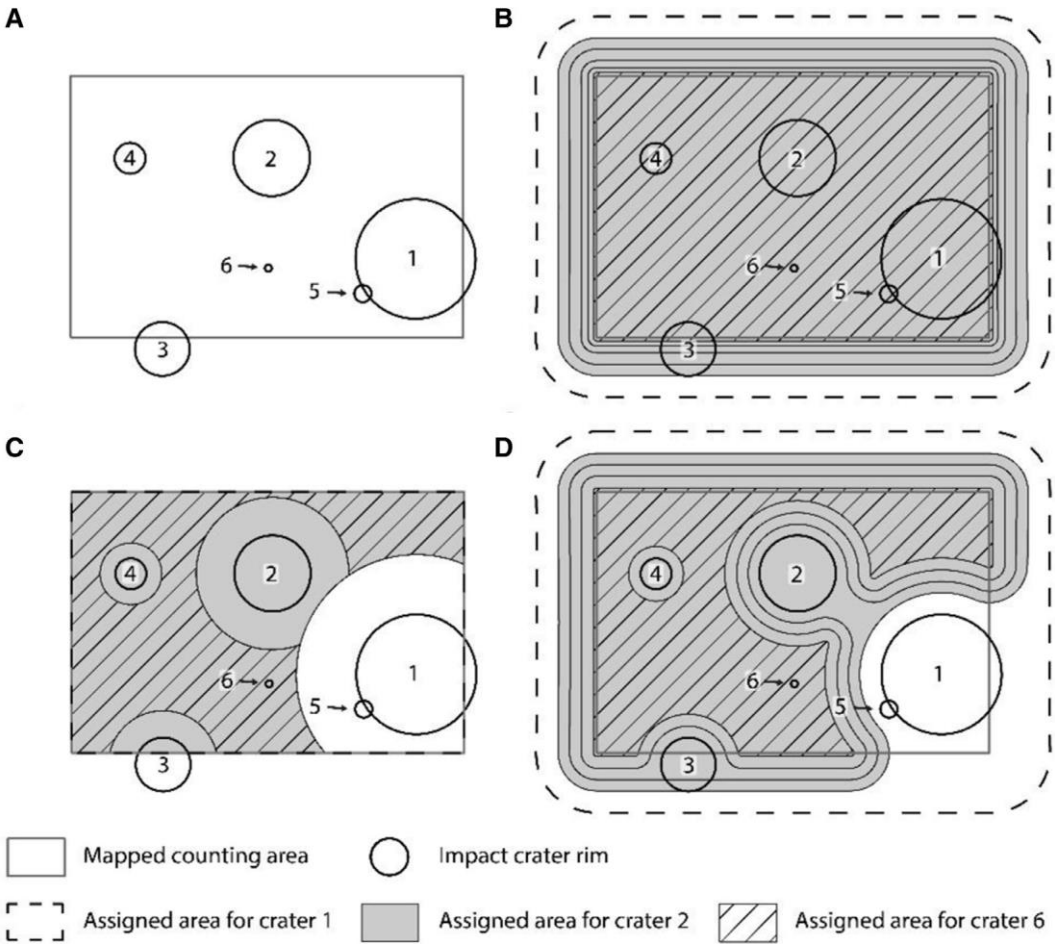

Fig. 1. Assignment of reference areas to individual craters. (A) Traditional crater counting approach. All craters use the same measurement area (grey outline). Crater 3 is excluded from the measurement because its crater center is located outside the counting area. (B) Buffered crater counting (BCC) approach. All craters are used for the analysis. The assigned measurement areas for each crater correspond to the original counting area plus a surrounding buffer of 1 crater radius. (C) Non-sparseness correction (NSC). Removal of "resurfaced" areas (craters plus ejecta blankets) from the counting area assigned to each respective crater. The area assigned to crater 1 (dashed outline) corresponds to the original counting area. For the second largest crater, crater 2, the assigned area is reduced by the area of crater 1 plus its ejecta blanket (1 radius). The measurement area assigned to crater 6 (striped area) excludes the crater and ejecta areas of all larger craters. Crater 5 is excluded from this measurement because it is located in the area resurfaced by crater 1. Crater 3 is excluded from the measurement too because its crater center is located outside the counting area. (D) Buffered non-sparseness correction (BNSC). Combination of B and C. In a first step, the resurfaced areas (craters plus ejecta blankets) are excluded from the counting areas assigned to each respective crater. Subsequently, we apply a buffer with the width of 1 crater radius. Crater 5 is excluded from this measurement because it is located in the area resurfaced by crater 1. Crater 3 however is included because its crater rim intersects the counting area.

Using the buffered crater counting (BCC) approach (for details see Tanaka, 1982 ; Fassett and Head, 2008 ; Hoke and Hynek, 2009 ; Kneissl et al., 2015), the statistics of a CSFD measurement can be improved by also including the craters whose centers are located outside the counting area, but whose crater rims or ejecta blankets still cut the boundary of the area (Fig. 1 B). In the BCC technique, every crater gets assigned an individual reference area, A_i , which consists of the area of the geologic unit, A_U , plus a specific buffer area, B_i , with the width of at least one crater radius around the geologic unit:

$$A_i = A_U + B_i$$

For details on different buffer widths depending on the usage of ejecta blankets see Kneissl et al. (2015) .

On heavily cratered surfaces pre-existing craters are often erased or covered by subsequent impacts. This is due to the impact event itself, the emplacement of a continuous ejecta blanket, and potentially the seismic shaking (e.g., Titley, 1966 ; Schultz and Gault, 1975 ; Richardson et al., 2005 ; Thomas and Robinson, 2005). As mentioned above, this eliminates a portion of the accumulated smaller craters in the measured CSFD of the surface. For larger crater sizes this effect is reduced, because it is less likely that these craters are completely obliterated by subsequent smaller craters. Due to the size-dependent effect of this process, we expect a change of the shape of the resulting CSFDs, typically a flattening of the CSFD curve (in a cumulative plot), complicating the inter- pretation and age extraction.

Here, we account for the influence of obliteration by subsequent impacts by removing the surface area covered by all craters larger than the crater currently under consideration. This also includes their corresponding continuous ejecta blankets, which have to be excluded from the assigned counting area, too (Fig. 1 C). In principle, one could remove the areas of all impact craters, smaller and larger, within the counting area and use the remaining area as measurement area. However, due to the fact that smaller craters cannot normally obliterate larger craters, only the areas of larger impact craters must be excluded. We note that this procedure could also diminish the effects of so-called auto-secondary cratering (see e.g., Zanetti et al., 2015). In the proposed technique, hereafter called non-sparseness correction (NSC), the assigned

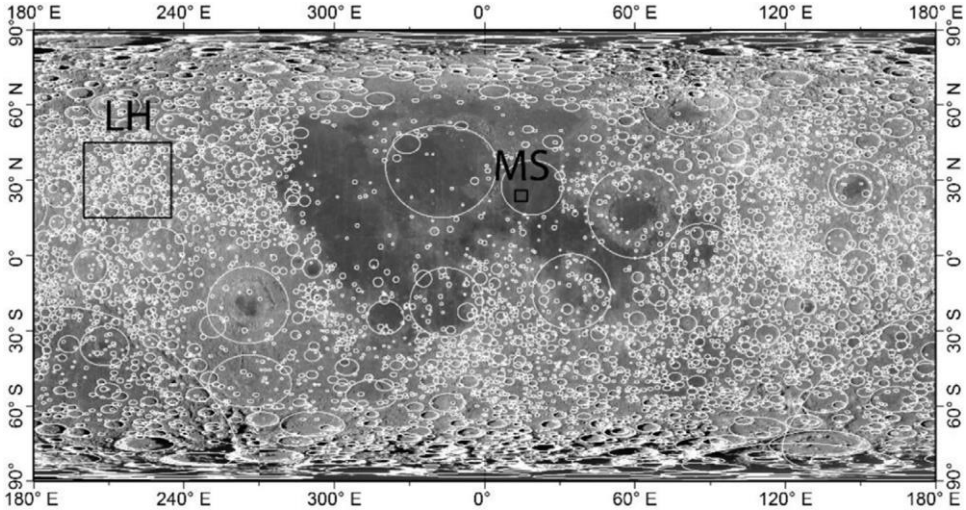

Fig. 2. Global map of the Moon showing the locations of the two sample regions (black rectangles), one in the Mare Serenitatis (area MS) and one in the lunar highlands
(area LH), as well as the lunar crater catalog (white circles) from Head et al. (2010) containing all impact craters and basins larger than 20 km in diameter. Base map is a
global mosaic of LROC WAC image data in a simple cylindrical map projection.

individual counting areas to each crater can be calculated using the following formula:

$$A_i = A_U - A_U \cap \bigcup_{j=1}^{i-1} (A_C + A_E)_j$$

where A i is the reference area assigned to a specific crater diam- eter, A U is the area of the geologic unit of interest, A C is the area covered by the crater j , and A E is the area covered by its ejecta blanket. In this approach the craters are sorted by diameter in de- creasing order, i.e., with increasing i and j the craters decrease in size.

Since the morphologies and extents of continuous ejecta blan- kets vary between different locations on a planetary body and likely depend on the properties of the different geological units, the radial extent of the ejecta area which is excluded in the new technique should be defined for each counting area separately. We propose to define this value by determining the average ra- dial ejecta extent of the most-pristine large craters in the counting area. The extent of the ejecta blankets of these fresh craters pro- vide a reasonable proxy for the former extent of the ejecta blan- kets of all craters in the counting area, even for the heavily de- graded ones. In this respect we want to emphasize that even if ejecta blankets of older craters are not visible any more, their ar- eas still have to be excluded from the assigned counting area be- cause they potentially obliterated preexisting craters during their formation process. This modifies the resulting CSFD of the overall geologic unit even if the crater density difference might not be ob- vious in the counting area. Here, the exclusion of these areas is not problematic in a statistical sense because impact cratering repre- sents a completely random process. The only disadvantage of this procedure is the reduced number of craters which can be used for the analysis.

Another important point is the size-dependent capability of ejecta blankets to obliterate craters. One might think that thin ejecta cannot cover relatively large craters and, thus, the ejecta area must not be excluded for all craters with respectively smaller diameters. However, since preexisting craters might be filled or simply heavily degraded when they are covered, even relatively large craters might not be identified in a count when they are covered by thin ejecta. Thus, we recommend to exclude the ejecta area for all crater sizes smaller than the crater currently under consideration.

In order to improve statistics, the new approach can be com- bined with the BCC technique (Fig. 1 D). Merging both approaches allows the inclusion of craters whose centers are located outside the counting areas, but whose crater rims cut the boundary (crater 3 in Fig. 1). This accounts also for craters whose centers are cov- ered by ejecta blankets, but which are still identifiable by the re- maining portion of their rim. In the combined approach, which hereafter will be called the buffered non-sparseness correction (BNSC), the reference area assigned to a specific crater diameter A i corresponds to the reference area from the NSC approach given in the formula above plus a buffer area, B i , with the width of at least 1 radius surrounding the reference area, i.e.,

$$A_i = A_U - A_U \cap \bigcup_{j=1}^{i-1} (A_C + A_E)_j + B_i$$

3. Case studies

3.1. Test Site Selection

To demonstrate the new approach and its effect on the derived CSFDs of differently aged geologic units, we chose two sample ar- eas on the Moon, one on the relatively young, sparsely cratered Mare Serenitatis (area MS) and one on the ancient lunar highlands (area LH).

The test area MS is a rectangle located between 12–17 °E and 21.5–26 °N (Fig. 2) covering a relatively lightly cratered and rela- tively homogenous albedo region on the floor of Serenitatis. Impact craters are well separated from each other allowing easy identifi- cation. Obvious secondary crater clusters were excluded from the counting area (see Fig. 3).

Area LH is a rectangle located between 200–235 °E and 15–45 °N in the lunar highlands (Fig. 2). This region was selected because it is one of the prime examples for non-sparsely cratered regions on the Moon. Here, the main geologic process is impact cratering. Since the lunar production function (PF) from Neukum (1983) is only defined for the diameter range between 10 m–300 km and the derived CSFDs will be compared to this PF, we selected a re- gion of the lunar highlands which exhibits a low density of impact basins, i.e., impact structures > 300 km in diameter. The only im- pact basin which intersects with the test site is the basin Dirichlet- Jackson whose rim covers the south-eastern corner of the counting area.

3.2. Data and methods

For area LH we used the lunar impact crater catalog as pro- vided by Head et al. (2010) (Fig. 2). This catalog is based on topographic data derived by the Lunar Orbiter Laser Altimeter (LOLA, Smith et al., 2010), onboard the Lunar Reconnaissance Or- biter (LRO) spacecraft and contains all impact craters and

basins ≥20 km. Since this catalog does not contain craters smaller than 20 km, all results derived from its analysis are unlikely to be af- fected be secondary cratering effects (Wilhelms et al., 1978; Head et al., 2010; Fassett et al., 2012).

Since the relatively young Mare Serenitatis does not contain craters ≥20 km, we performed our own crater measurements on area MS. Here, we used a mosaic from the LRO Wide Angle Camera (WAC; Robinson et al., 2010) with a spatial resolution of 100 m/pixel. Craters were measured down to a diameter of ~500 m. All crater measurements were carried out in a GIS envi- ronment (ESRI ArcGIS) using the CraterTools add-in (Kneissl et al., 2011). Besides traditional crater counting, this software allows the application of the buffered crater counting (BCC) approach (e.g., Fassett and Head, 2008; Kneissl et al., 2015). Furthermore, we adapted the software to allow for the application of the NSC and BNSC approaches, i.e., for the systematic exclusion of crater and ejecta blanket areas. CSFD data were plotted and analyzed us- ing the CraterStats software (Michael and Neukum, 2010; Michael, 2013). Here, we follow the recommendation of Arvidson (1979) and show both, the cumulative plot with a pseudo-log crater bin- ning as well as the relative representation (R plot) with a coarser 10/decade crater binning.

The measurements for both areas, MS and LH, were analyzed using the 4 different approaches mentioned above: (1) the tradi- tional crater counting approach, (2) the BCC approach, (3) the NSC approach, and (4) the BNSC approach (NSC combined with BCC).

As mentioned above, we defined the radial extent of the ejecta blanket, whose area is excluded from the respectively assigned areas in the NSC and BNSC approaches, by looking at the ex- tent of the continuous ejecta blankets of the pristine large craters in the region of the counting area. In both areas, MS and LH, we observed an extent of approximately one crater radius ra- dial from the crater rim. This extent of continuous ejecta is con- sistent with typical values given for the Moon, e.g., by Melosh (1989) .

To compare the results with each other and with the shape of the lunar PF we fitted the given PF from Neukum (1983) to the measured cumulative CSFD data in the usual manner. The resulting theoretical N (1) value, i.e., the frequency of craters ≥1 km, allows the extraction of a cratering model age from the lunar chronology function (CF) (Michael and Neukum, 2010). For comparison we also display the isochron of the derived age, i.e., the vertical position of the PF, in the R plot of each measurement.

3.3. Results and interpretation

3.3.1. Mare Serenitatis

Craters on area MS are sparsely distributed over the surface and show almost no overlap (see Fig. 3). In the traditional crater analysis the crater bins nicely follow the given lunar PF, this applies for both, the cumulative and the R plot representations (Fig. 4 A and B). The resulting age is 2.64 + /–0.12 Ga. Only the two smallest crater bins deviate from the PF, which is explained by the “roll

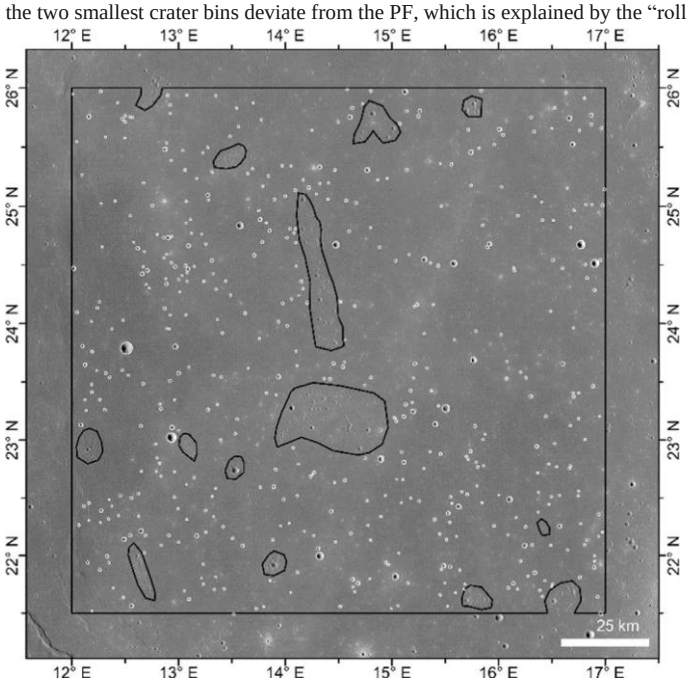

Fig. 3. Test area on Mare Serenitatis (area MS). Mapped impact craters are marked as white circles. The outline of the counting area is marked in black. Obvious sec- ondary crater fields were excluded from the counting area. Basemap is LROC WAC mosaic (100 m/pixel) in Mercator map projection .

over” caused by the limit of image resolution (only crater sizes < 500 m are affected).

Looking at the results from area MS (Fig. 4), none of the ap- plied corrections changed the CSFD in a way that it deviates from the shape of the PF in a noticeable way. This is due to the fact that the crater sizes are relatively small compared to the total area and, consequently, the difference between the buffered areas and the original counting area is negligible: the craters are sparse. Fur- thermore, the areas removed due to crater and ejecta coverage are relatively small and almost no craters were excluded from the analyses due to direct overlapping. The total number of craters ex- tracted from the measurement varies only by a few craters for the different applied corrections (traditional: 497, BCC: 499, NSC: 493, BNSC: 497, see also Fig. 4).

Nevertheless, since the different applied corrections slightly change the reference areas, the absolute ages derived from the CF vary as well. Note that the areas given in the plot legends of all CSFD plots for the test areas MS and LH represent the area of the originally mapped counting area. The respective areas used for the calculation of the crater frequencies of the individual diameter bins (BCC, NSC and BNSC approaches) vary from bin to bin as described above.

In the BCC approach, all assigned areas are slightly larger than the area originally mapped. Consequently, the derived age (2.57 + 0.11/–0.12 Ga, Fig. 4 C/D) is lower than for the traditional crater analysis (2.64 + /–0.12 Ga, Fig. 4 A/B).

Applying the NSC, only the largest crater gets assigned the full measurement area. The measurement areas assigned to all the smaller crater sizes are slightly reduced, shifting the bins faintly upwards. This does not change the shape of the resulting CSFD in a noticeable way but the resulting age is increased compared to the traditional counting approach (2.68 + /–0.12 Ga, Fig. 4 E and F).

The BNSC approach (Fig. 4 G and H) represents the combination of the NSC and BCC approaches. Consequently, the assigned areas are reduced in a first step (removal of the areas of the

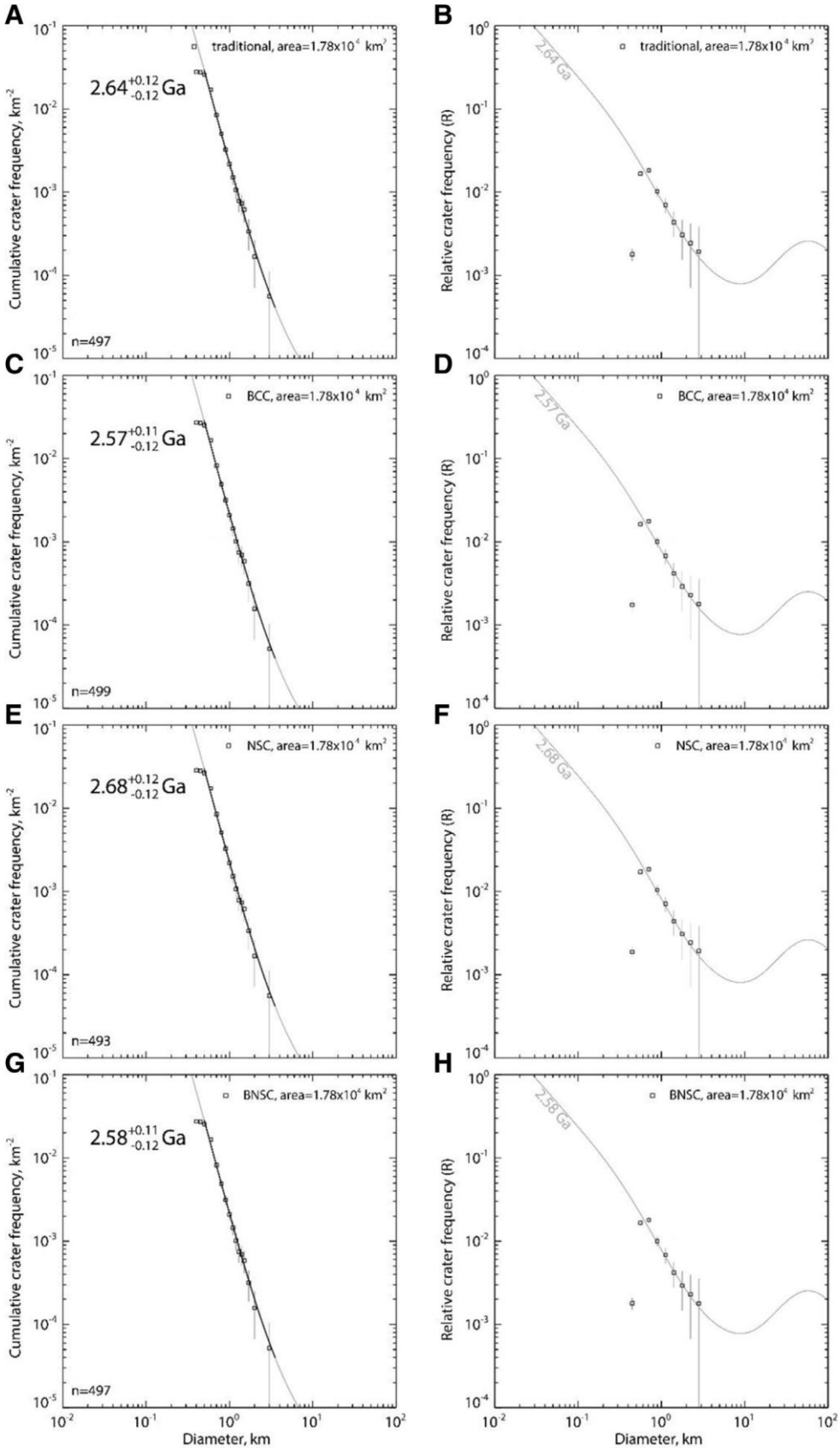

Fig. 4. CSFDs derived from Mare Serenitatis (area MS). All results are shown in cumulative (left) and R plot (right) representations for the (A/B) traditional crater counting approach, (C/D) buffered crater counting (BCC) approach, (E/F) non-sparseness correction (NSC) approach, and (G/H) buffered non-sparseness correction (BNSC) approach. The area given in the plot legends is the area of the mapped counting area. The actual areas used for the calculation of the crater bin frequencies vary from bin to bin (in the BCC, NSC and BNSC approaches) as described in the main text.

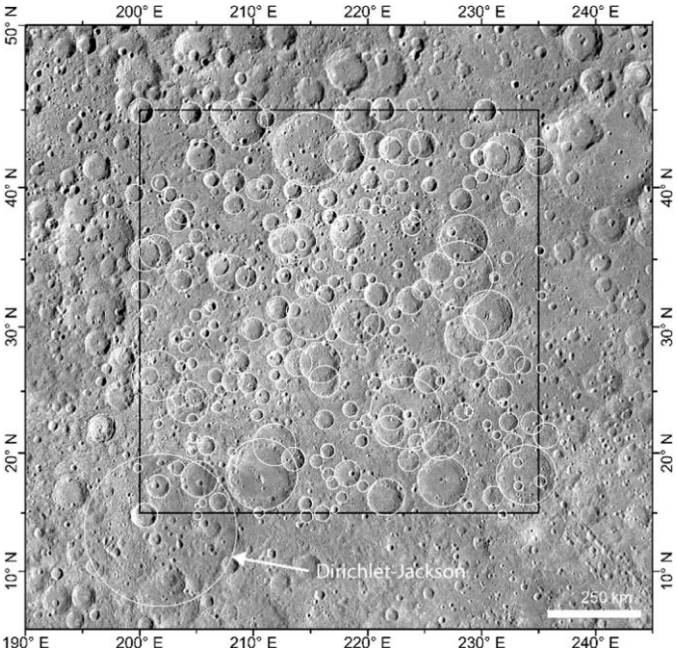

Fig. 5. Test area on the lunar highlands (LH). Impact craters (white circles) are taken from the lunar crater catalog from Head et al. (2010) containing craters ≥ 20 km. The outline of the counting area is marked in black. Basemap is LROC WAC mosaic (100 m/pixel) in Mercator map projection.

respectively larger craters), which increases the resulting age (NSC approach). In the second step, however, the respectively assigned areas get enlarged by the buffering process which, in this case, leads to a decrease of the resulting age. In the case of the sparsely- cratered test site MS, the area-enlargement effect of the buffer- ing process is stronger than the area-reduction effect of the re- moval of the respectively larger craters. Thus, the derived age (2.58 + 0.11/–0.12 Ga) is lower than for the traditional crater counting or the NSC approaches, but still slightly higher than for the BCC ap- proach. As mentioned above, the addition or subtraction of addi- tional craters from the measurement plays only a minor role for sparsely cratered counting areas.

3.3.2. Lunar highlands

Test area LH is a non-sparsely cratered surface where the ob- served impact craters often overlap each other (see Fig. 5). Larger craters can be either superposed by several other large craters or appear relatively pristine, e.g., the one north-east of the Dirichlet- Jackson basin.

In the traditional crater counting approach, of the 195 craters identified in the crater measurement, 16 were excluded because their centers are located outside the counting area. The CSFD derived using the traditional approach (Fig. 6 A and B) fits the given PF only at the larger crater diameter bins (∼70–170 km). The portion of the CSFD curve left of, i.e, smaller than, ∼70 km is noticeably flatter than the given PF in the cumulative data representation. The model age derived from the larger craters – those craters which would normally be used to find an age – is 4.31 + /–0.03 Ga, fitting 23 craters.

The application of the BCC approach adds another crater bin at the large end of the CSFD; Dirichlet-Jackson basin is included in the measurement, because it extends partly into the measurement area. A number of other craters on the boundary of the count area are also now included in the analysis. The total number of craters used in the BCC approach is 211. However, the shape of the curve does not change noticeably compared to the traditional counting approach. Instead of an increase of the resulting age, which could be expected due to the addition of craters, we observe a slight decrease of the derived age due to the buffer-related increase of the counting areas. The age, however, is still within the error of the age from the traditional approach: 4.28 + /–0.03 Ga, fitting 24 craters.

After the application of the NSC technique the CSFD is notice- ably steeper in the diameter range ≤70 km. The CSFD can be fit- ted by the PF over almost the entire diameter range (except the smallest crater bin, 20 km). The exclusion of craters within respec- tively larger craters and their ejecta led to the reduction of the to- tal number of craters used in the measurement. Only 57 craters are left after the correction. However, almost all of them (52) can be used for the fit of the PF. At the same time, the statistical noise in- creases significantly in the NSC approach due to the smaller num- ber of craters per bin. This is visible in particular in the R plot representation of the CSFD data (Fig. 6 F). The resulting model age is 4.28 + /–0.02 Ga.

The application of the BNSC technique, i.e., the combination of the NSC and BCC approaches, yields 88 craters for the measure- ment. This again includes the Dirichlet-Jackson basin, as it cuts the boundary of the counting area. As in the NSC approach, the re- sulting CSFD curve can be fitted almost over the entire diameter range. However, due to the addition of buffering, the total number of craters which can be used in the fitted diameter range is notice- ably higher than in the NSC approach alone (78 vs. 52). This leads to less noise in the CSFD curve, as seen in the R plot (Fig. 6 H). The resulting age after the application of the BNSC technique is 4.27 + 0.01/–0.02 Ga.

4. Summary and discussion

The application of the four different techniques to area MS demonstrated that all of the approaches produce similar CSFD curves for young sparsely-cratered surfaces. To demonstrate how similar the CSFDs are, we plotted all derived CSFD data in a sin- gle diagram (Fig. 7 A and B) which show almost no vertical shift or exclusion of crater bins. Here, all model ages derived from mea- surement area MS show overlapping error bars (Fig. 4 A,C,E,G).

In contrast to the results from area MS, the application of the four approaches to area LH reveals a clear change between the re- sulting CSFD curves, in particular in the smaller diameter range (Fig. 7 C and D). The proposed BNSC approach allows fitting the lu- nar PF over a larger diameter interval than the traditional crater counting approach and the BCC approach. At the same time, the BNSC approach uses a larger number of craters per bin compared to the NSC technique. This decreases the statistical noise and, thus, allows for a more reliable age determination of ancient, non- sparsely cratered surfaces. Fig. 8 shows a comparison of the un- corrected (traditional) CSFD curve and the curve derived using the BNSC approach. In the lower panels we additionally plotted the re- spective deviations from the fitted PF (black solid lines in the up- per panels). The RMS error derived from the traditional approach (0.137) is significantly higher than the RMS error from the BNSC approach (0.063) indicating a much better agreement of the cor- rected CSFD with the PF.

With the application of the BNSC technique, the derived CSFD allows for a more confident age extraction, making use of a wider range of crater diameters which conform to the same isochron, providing an age of 4.26 Ga (Fig. 8 B).

The small-diameter craters in the traditional approach might have suggested a much younger age for the surface (4.20 Ga isochron in Fig. 8 A) than the large crater diameters (4.31 Ga isochron in Fig. 8 A) although we note that we would have tended to treat the largest observed craters on a given unit as the most

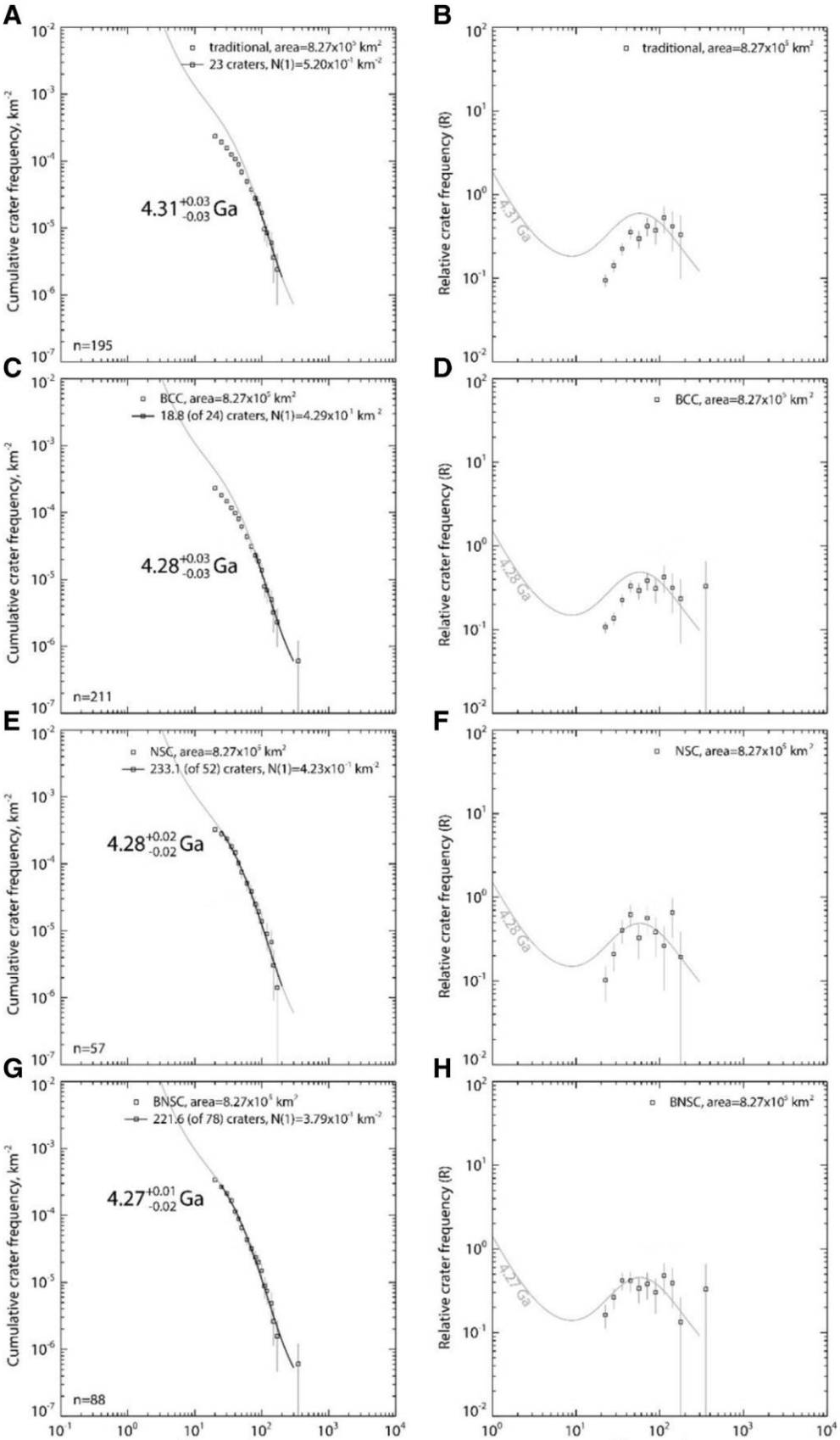

Fig. 6. CSFDs derived from the lunar highlands (area LH). All results are shown in cumulative (left) and R plot (right) representations for the (A/B) traditional crater counting approach, (C/D) buffered crater counting (BCC) approach, (E/F) non-sparseness correction (NSC), and (G/H) buffered non-sparseness

correction (BNSC) approach. The area given in the plot legends is the area of the mapped counting area. The actual areas used for the calculation of the crater bin frequencies vary from bin to bin (in the BCC, NSC and BNSC approaches) as described in the main text.

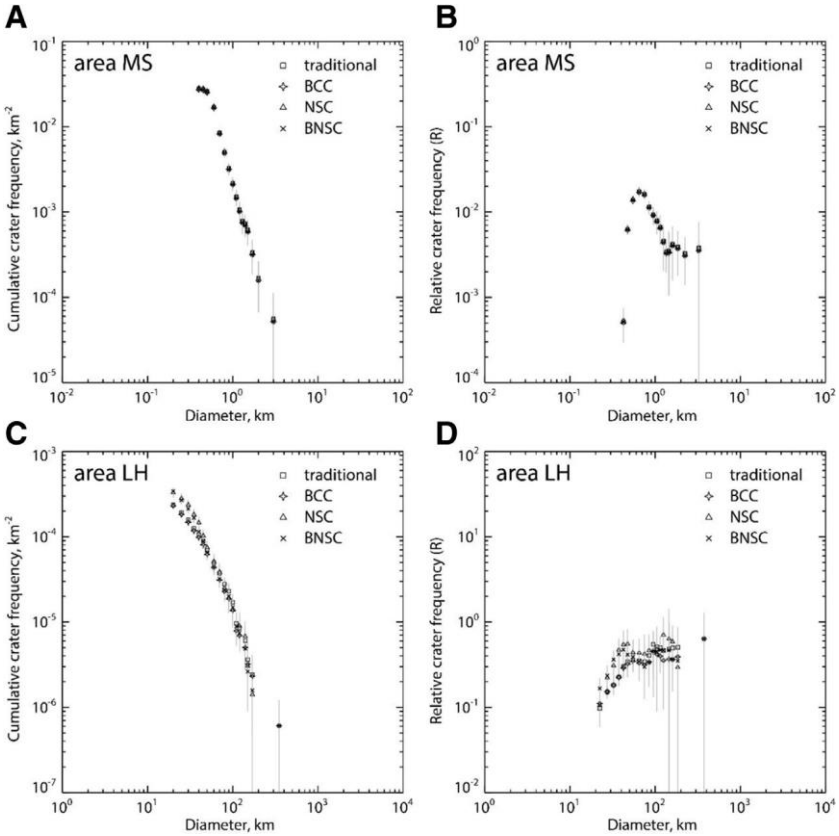

Fig. 7. Comparison of the effects of the applied correction techniques between (A/B) the sparsely cratered surface area MS and (C/D) non-sparsely cratered surface area LH

in cumulative and R plot representations, respectively.

reliable for determining an age. This is, in part, because the largest craters are always sparse.

We see that the new technique is useful because, firstly, it al- lows us to better understand and interpret what we see in the crater populations, and secondly, when we are trying to examine the shape of the production function itself, it enables us to ob- tain broader contiguous ranges of the size–frequency distribution. In constructing a complete production function for a chronology model (Neukum, 1983) a piecewise normalization is required: the larger the pieces which are used, the better constrained is the final function.

Interestingly, the results from our test area on the lunar high- lands also indicate that the actual shape of the CSFDs on the an- cient surfaces of the Moon are still in agreement with the lunar PF from Neukum (1983) even down to craters of diameter 20 km. This appears to contradict studies by, e.g., Strom et al. (1988), Strom et al. (2005), Head et al. (2010) , or Fassett et al. (2012) , who found that CSFDs on the ancient lunar highlands are significantly differ- ent from the shapes of the CSFDs superposed on younger lunar surfaces. Further work is underway to investigate this important finding in more detail.

4.1. Restrictions of the BNSC technique

Since the crater catalog used for the study of area LH is lim- ited to craters > 20 km in diameter, it is unlikely that secondary craters affected our results significantly (Head et al., 2010; Fassett et al., 2012). However, when investigating smaller crater diameters it is still important to exclude obvious clusters of secondary craters during the crater mapping process.

The proposed BNSC approach allows us to remove the influence of crater superposition. Other potential resurfacing processes, e.g., volcanic activity, eolian erosion, or mass wasting cannot be cor- rected by the techniques presented in this work, no matter if it affected the whole counting area or just parts of it. Consequently, it is still necessary to use counting areas that correspond to homo- geneous geological units, i.e., units and their materials that were formed or modified by the same geologic process (e.g., Wilhelms et al., 1987).

When investigating smaller counting areas, where for instance one or two large craters and their ejecta blankets cover large parts of the counting area, the new technique is not capable of elim- inating the statistical influence of the one or two large craters. Consequently, the corrected CSFD might still be ambiguous for an age extraction. In such a case, we would recommend reducing the original counting area, excluding the influence of the one or two large craters and just analyzing the unaffected (not covered) small craters.

As a final note, it is worth mentioning that non-sparseness is associated with, though starting well before, the beginning of a condition called “crater equilibrium”, sometimes also “saturation equilibrium” or just “saturation”, where due to the spatial den- sity of the craters for each new crater formed, a crater of ap- proximately the same size is erased (e.g., Gault, 1970 ; Hartmann, 1984 ; Richardson, 2009). Since the BNSC approach excludes ar- eas which are covered by larger craters or their ejecta blankets, the application of the BNSC technique will typically exclude crater sizes which are affected by saturation effects. As a result the corresponding crater bins will not appear on the derived CSFD plots.

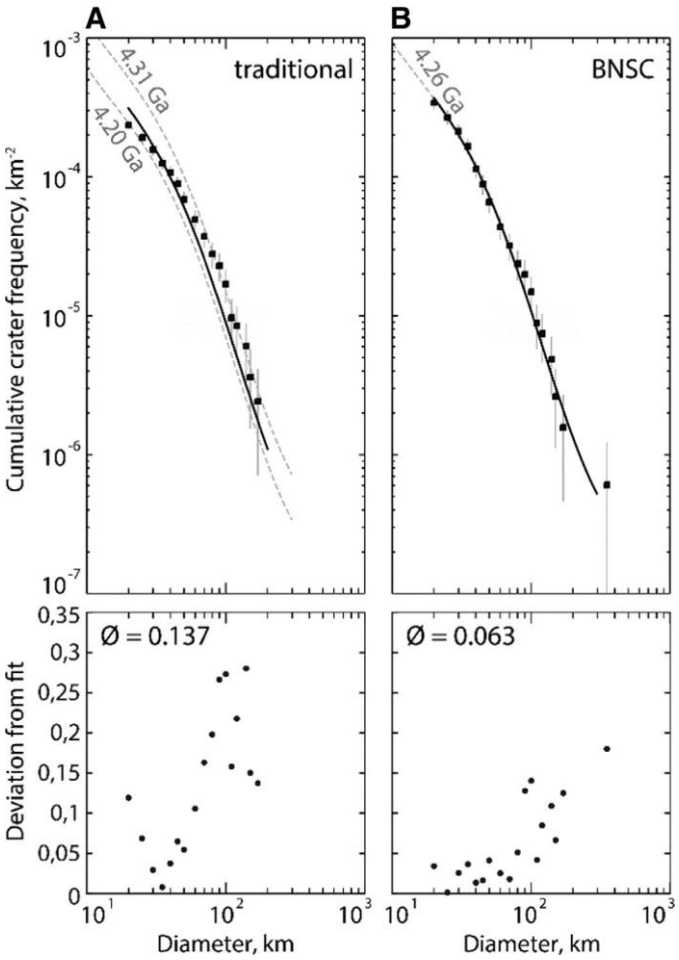

Fig. 8. Fit errors on (A) uncorrected (traditional) and (B) corrected (BNSC) CSFDs. Lower panels show the respective deviation from the lunar PF which was fitted over the whole diameter range (solid black lines in the upper panels). Isochrons shown in the upper left panel (traditional) correspond to ages from data fits of the three smallest bins (4.20 Ga isochron) and the original fitting range of the larger crater bins (4.31 Ga isochron, see Fig. 6 A). The isochron shown in the upper right panel (BNSC) corresponds to the age derived from the data fit over all crater diameters.

5. Conclusions

The proposed correction of non-sparsely cratered surfaces suc- cessfully accounts for the loss of craters due to subsequent crater/ejecta coverage.

The correction extends the crater diameter range that can be used for fitting the lunar PF, and thus, allows for more confi- dent age determinations.

Thus, we highly recommend general application of the new buffered non-sparseness correction (BNSC) to extract CSFDs from measurements on non-sparsely cratered surfaces.

The algorithm has only a minor effect on young, sparsely cratered surfaces such as the lunar maria.

The application of our new technique hints that the shape of the CSFDs on the lunar highlands might be very similar to the shape of the lunar PF from Neukum (1983), in contrast to the findings of, e.g., Strom et al. (2005), Head et al. (2010) , or Fassett et al. (2012) .

Acknowledgments

This work was partly supported by the German Research Foun- dation (DFG) SFB TRR-170-1 TP A3 and TP A4 and the DLR Space Administration on behalf of the Federal Ministry for Economic Af- fairs and Energy, grants 50 QM 1301 (HRSC on Mars Express), and 50 OH 1503 (Cassini). We appreciate the suggestions of Carolyn van der Bogert and an anonymous reviewer which helped improve the manuscript.

References

Arvidson, R. , 1979. Crater analysis techniques working group – Standard techniques for presentation and analysis of crater size-frequency data. Icarus 37, 467–474 .

Baldwin, R.B. , 1964. Lunar crater counts. Astron. J. 69, 377–392 .

Fassett, C.I. , Head, J.W. , 2008. The timing of martian valley network activity: Con- straints from buffered crater counting. Icarus 195, 61–89 .

Fassett, C.I., Head, J.W., Baker, D.M.H., et al., 2012. Lunar impact basins: Stratigraphy, sequence and ages from superposed impact crater populations measured from Lunar Orbiter Laser Altimeter (LOLA) data. J. Geophys. Res. 117, E00L06. doi: 10. 1029/2011JE003951 .

Gault, D.E. , 1970. Saturation and equilibrium conditions for impact cratering on the lunar surface: Criteria and implications. Radio Science 5, 273–291 .

Hartmann, W.K. , 1984. Does crater 'saturation equilibrium' occur in the Solar Sys- tem? Icarus 60, 56–74 .

Head, J.W. , Fassett, C.I. , Kadish, S.J. , et al. , 2010. Global distribution of large lu- nar craters: Implications for resurfacing and impactor populations. Science 329, 1504–1507 .

Hoke, M.R.T., Hynek, B.M., 2009. Roaming zones of precipitation on ancient Mars as recorded in valley networks. J. Geophys. Res. 114, E08002. doi: 10.1029/20 08JE0 03247 .

Kneissl, T. , Michael, G.G. , Platz, T. , et al. , 2015. Age determination of linear sur- face features using the Buffered Crater Counting approach – Case studies of the Sirenum and Fortuna Fossae graben systems on Mars. Icarus 250, 384–394 .

Kneissl, T. , van Gasselt, S. , Neukum, G. , 2011. Map-projection-independent crater size-frequency determination in GIS environments – New software tool for Ar- cGIS. Planet. Space Sci. 59, 1243–1254 .

Melosh, H.J. , 1989. Impact Cratering: A Geologic Process. Oxford University Press, New York, p. 245 .

Michael, G. , Neukum, G. , 2010. Planetary surface dating from crater size-frequency distribution measurements: Partial resurfacing events and statistical age uncer- tainty. Earth Planet. Sci. Lett. 294, 223–229 .

Michael, G.G. , 2013. Planetary surface dating from crater size–frequency distribution measurements: Multiple resurfacing episodes and differential isochron fitting. Icarus 226, 885–890 .

Neukum, G., 1983. Meteoritenbombardement und Datierung planetarer Oberflächen, habilitation thesis. Ludwig-Maximilians Universität München, Fakultät für Ge- owissenschaften, München, p. 186 (English translation, 1984: Meteorite bom- bardment and dating of planetary surfaces.) http://ntrs.nasa.gov/search.jsp?R= 19840027189 .

Öpik, E.J. , 1960. The lunar surface as an impact counter. Mon. Not. R. Astron. Soc. 120, 404–411 .

Richardson, J.E. , 2009. Cratering saturation and equilibrium: A new model looks at an old problem. Icarus 204, 697–715 .

Richardson, J.E. , Melosh, H.J. , Greenberg, R.J , et al. , 2005. The global effects of im- pact-induced seismic activity on fractured asteroid surface morphology. Icarus 179, 325–349 .

Robinson, M.S. , et al. , 2010. Lunar Reconnaissance Orbiter Camera (LROC) instru- ment overview. Space Sci. Rev 150, 81–124 .

Schultz, P.H. , Gault, D.E. , 1975. Seismically induced modification of lunar surface features. In: Proceedings of the Lunar and Planetary Science Conference, 6, pp. 2845–2862 .

Smith, D.E. , Zuber, M.T. , Jackson, G.B. , et al. , 2010. The Lunar Orbiter Laser altimeter investigation on the lunar reconnaissance orbiter mission. Space Sci. Rev. 150, 209–241 .

Strom, R.G. , Malhotra, R. , Ito, T. , et al. , 2005. The origin of planetary impactors in the inner Solar System. Science 309, 1847–1850 .

Strom, R.G., Neukum, G., Chapman, C.R., et al., 1988 The Cratering Record on Mer- cury and the Origin of Impacting Objects. In: F. Vilas, (Ed.), Mercury, University of Arizona Press, pp. 336–373.

Tanaka, K.L. , 1982. A New Time-Saving Crater-Count Technique, with Application to Narrow Features. NASA, pp. 123–125 Technical Memo, NASA TM-85127 .

Thomas, P.C. , Robinson, M.S. , 2005. Seismic resurfacing by a single impact on the Asteroid 433 Eros. Nature 436, 366–369 .

Titley, S.R. , 1966. Seismic Energy as an Agent of Morphologic Modification on The Moon. Tech. Rep. United States Geological Survey, Flagstaff, AZ, p. 17 .

Warner, N.H. , Gupta, S. , Calef, F. , et al. , 2015. Minimum effective area for high reso- lution crater counting of martian terrains. Icarus 245, 198–240 .

Wilhelms, D.E. , McCauley, J.F. , Trask, N.J. , 1987. The geologic history of the Moon. U.S.. Geol. Surv. Prof. Paper, Report P 1348, p. 303 .

Wilhelms, D.E. , Oberbeck, V.R. , Aggarwal, H.R. , 1978. Size-frequency distributions of primary and secondary lunar impact craters. In: Proceedings of the Lunar and Planetary Science Conference Abstracts, 9, pp. 3735–3762 .

Zanetti, M. , Stadermann, A. , Jolliff, B.L. , et al. , 2015. Auto-Secondary cratering vs. tar- get property effects on ejecta blankets of copernican craters: What are the im- plications for age dating using small-diameter crater statistics? In: Proceedings of the Lunar and Planetary Science Conference, 46, p. 1209 .